Supporting Information

**Large Tunneling Magnetoresistance in van der Waals Ferromagnet/Semiconductor Heterojunctions**

Wenkai Zhu,[1,2] Hailong Lin,[1,2] Faguang Yan,[1] Ce Hu,[1,2] Ziao Wang,[1,2] Lixia Zhao,[1,7] Yongcheng Deng,[1,2] Zakhar R. Kudrynskyi,[3] Tong Zhou,[4] Zakhar D. Kovalyuk,[5] Yuanhui Zheng,[1,6] Amalia Patanè,[3] Igor Žutić,[4] Shushen Li,[1,2] Houzhi Zheng,[1,2] and Kaiyou Wang[1,2,6]*

[1]State Key Laboratory of Superlattices and Microstructures, Institute of Semiconductors, Chinese Academy of Sciences, Beijing 100083, China

[2]Center of Materials Science and Optoelectronics Engineering, University of Chinese Academy of Sciences, Beijing 100049, China

[3]School of Physics and Astronomy, University of Nottingham, Nottingham NG7 2RD, UK

[4]Department of Physics, University at Buffalo, SUNY, Buffalo 14260, US

[5]Institute for Problems of Materials Science, The National Academy of Sciences of Ukraine, Chernivtsi Branch, Chernivtsi 58001, Ukraine

[6]Beijing Academy of Quantum Information Sciences, Beijing 100193, China

[7]Tiangong University, Tianjin 300387, China

*Corresponding author. E-mail: kywang@semi.ac.cn

In order to probe the cleanliness of the interface between the FGT and InSe layers, we have conducted cross-section high-resolution transmission electron microscopy (HRTEM) studies. As shown in the HRTEM image of Figure S1, our studies show that the interface is atomically flat with the atomic layers in InSe and the FGT clearly visible. This excludes a significant contamination of the layers and their interface.
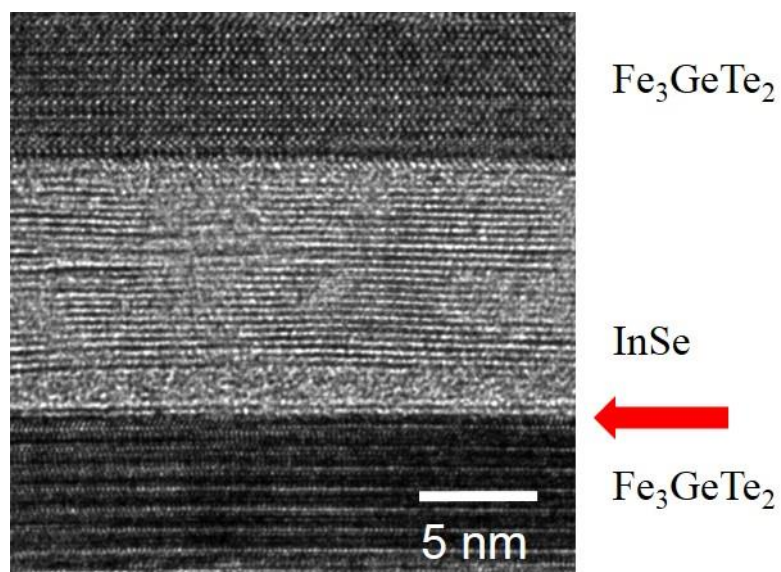


Figure S1. Cross-sectional high-resolution transmission electron microscopy (HRTEM) image of the FGT/InSe heterostructure and its interface marked by the red arrow.

Figure S2a presents the photoluminescence (PL) spectrum of a 6-nm-thick InSe flake at room temperature (*RT*) excited by a 532 nm laser, indicating that the bandgap is 1.39 eV, which is in good agreement with previous experimental results.[1] The *RT* Raman spectrum of the InSe flake with excitation wavelength $\lambda$ = 532 nm is shown in Figure S2b. The spacer InSe has 3 out-of-plane modes: $A'_1(1)$ at ~115 cm$^{-1}$, $A''_2(1)$ at ~200 cm$^{-1}$ and $A'_1(2)$ at ~228 cm$^{-1}$, and one in-plane $E''(2)$ mode at ~178 cm$^{-1}$, which is consistent with previous Raman studies on bulk γ-rhombohedral InSe.[2] These basic characterizations indicate that our InSe spacer layer has a good crystal quality.
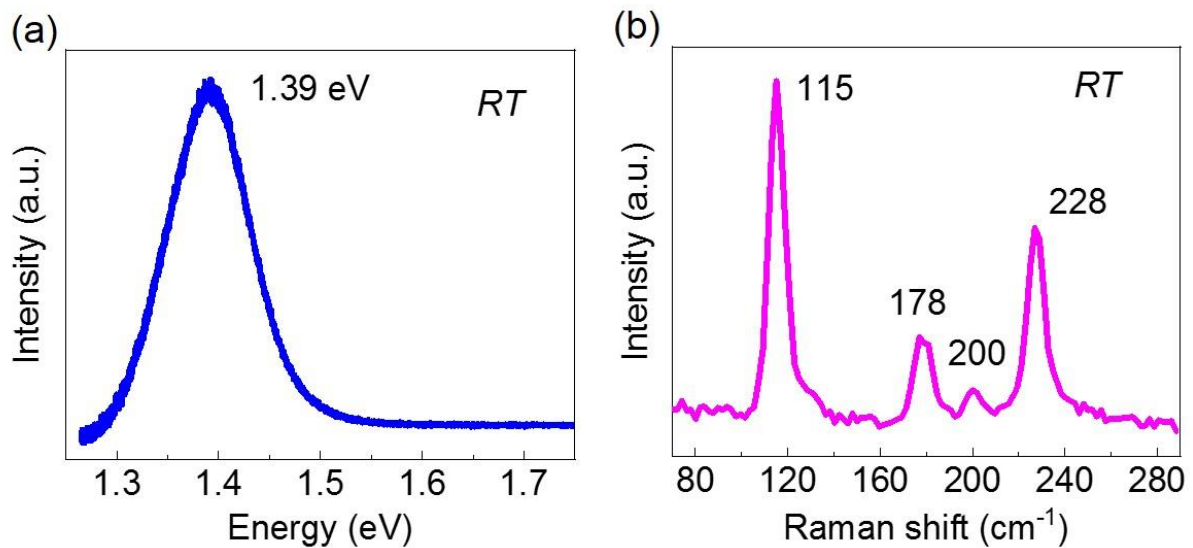


Figure S2. PL and Raman spectra of 6-nm-thick InSe. a) PL spectra of the InSe flake at room temperature (*RT*) excited by a 532 nm laser indicating a bandgap energy of 1.39 eV. b) Raman spectra of the InSe flake at *RT* and laser excitation wavelength $\lambda$ = 532 nm. The Raman peaks are centered at 115, 178, 200, and 228 cm$^{-1}$ and are consistent with previous Raman studies on bulk γ-rhombohedral InSe.
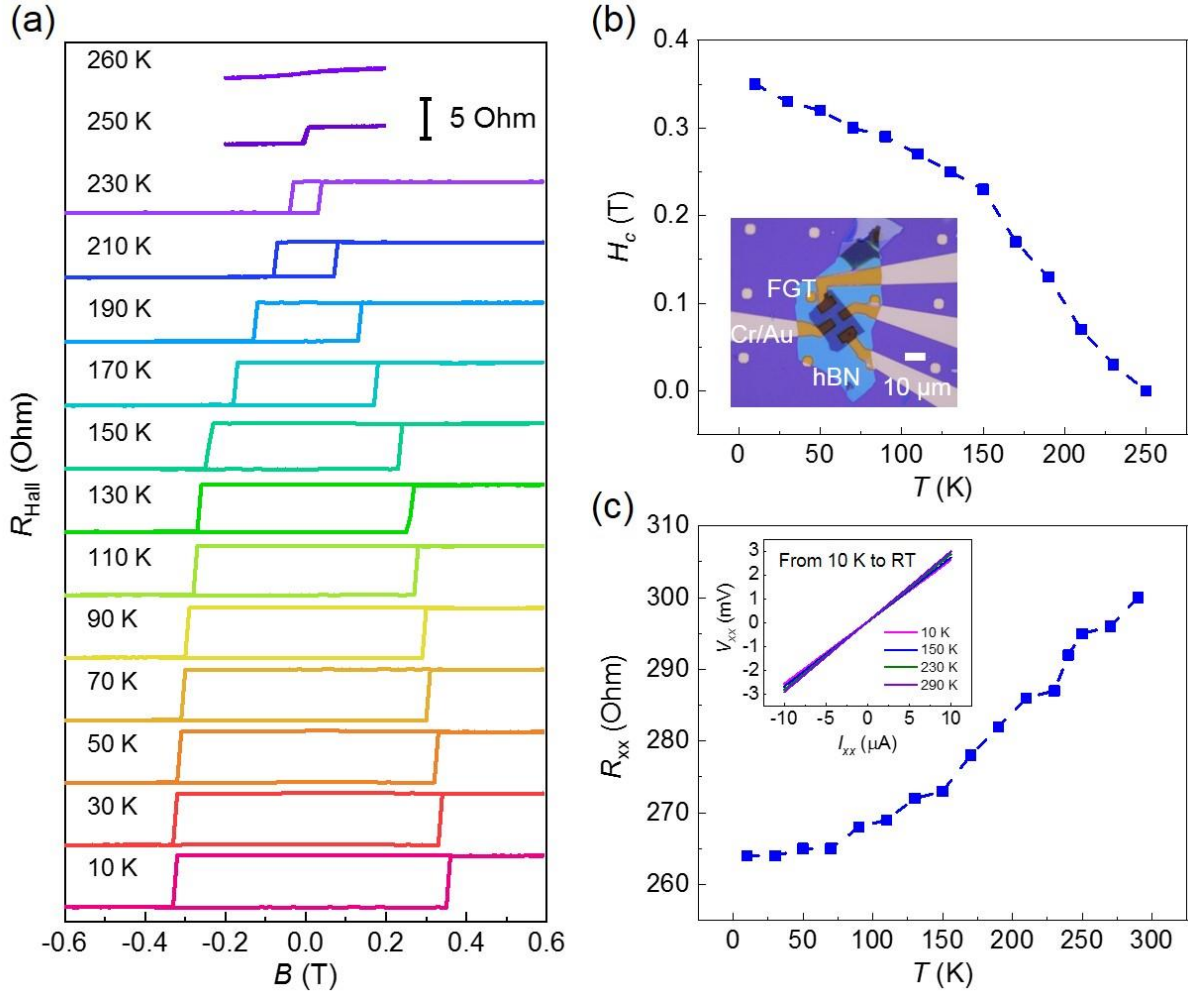
Figure S3. Anomalous Hall Effect (AHE) measurements of 15-nm-thick $Fe_3GeTe_2$ (FGT). a) Anomalous Hall resistance of a 15-nm-thick FGT Hall-bar device at various temperatures from 10 to 260 K. b) The corresponding coercivities as a function of temperature. The inset is an optical image of the Hall-bar device (the scale bar is 10 μm). c) Temperature dependence of the longitudinal resistance $R_{xx}$. The inset is the $I_{xx}$-$V_{xx}$ curves at different temperatures.

In order to characterize the magnetism of FGT, we measured the anomalous Hall signals of the FGT. Figure S3a shows the temperature-dependent Hall signals of a 15-nm-thick FGT device with out-of-plane magnetic field (**B**). The square-shape hysteresis loops indicate its perpendicular magnetic anisotropy (PMA), which persists up to 230 K. The Curie temperature ($T_c$) of the FGT device is similar to that reported in the bulk.[3] The $T_c$ and local magnetic moment of the FGT are related to the lattice quality. It decreases with the creation of Fe vacancies and the decrease of the in-plane lattice parameter.[4] We extracted the temperature-

dependent coercivities from the AHE results. As shown in Figure S3b, these decrease as the temperature increases. We also measured the temperature dependence of the longitudinal resistance (Figure S3c), which increases with increasing temperature in the measured temperature range, thus exhibiting metallic characteristics. The original $I_{xx}$-$V_{xx}$ curves of the Hall-bar device are shown in the inset of Figure S3c. The AHE results show that the exfoliated FGT flake is a 2D metallic ferromagnet with strong PMA and relatively high $T_c$, which verifies that the FGT flake has good crystal quality.
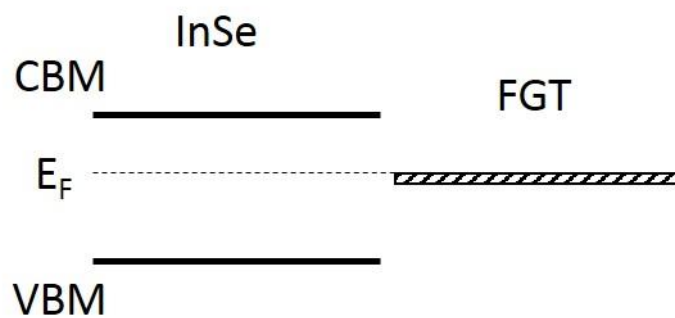


Figure S4. The relative positions of the conduction band minimum (CBM) and valence band maximum (VBM) of InSe and the Fermi energy level ($E_F$), indicating a Schottky barrier between the FGT and InSe.

Zhang et al. have performed density functional theory (DFT) calculations to model FGT/InSe/FGT magnetic tunnel junctions (MTJs).[5] These indicate that the conduction band minimum of monolayer InSe is higher than the Fermi level of the FGT by about 0.35 eV, leading to a Schottky barrier at the FGT/InSe interface. Figure S4 sketches the relative positions of the conduction band minimum and valence band maximum of monolayer InSe and the Fermi energy level. The FGT/InSe/FGT MTJs have been predicted to behave as perfect spin-filters with a giant TMR ratio of up to 700%. This originates from the unique band structure of InSe and its close match to FGT. A large spin-polarized transmission was assigned to evanescent states with Δ1-symmetry in InSe that are close to the Fermi level of the FGT electrodes. Referring to the spin-polarized band structure of FGT, the bands close to Fermi-level have also Δ1 symmetry, providing matching to the InSe states. Thus, InSe showed a Δ1-symmetry spin filter for FGT electrodes that is similar to the traditional spin filtering effect of a MgO barrier

with Fe electrodes, which has been extremely successful in MTJs and responsible for a huge increase in the observed TMR.[5] The tunneling probability of the electron throughout the semiconductor interlayer decays exponentially as $T(E_F) = Ae^{(-2KL)}$, where $K$ is the decay coefficient and $L$ is tunneling thickness.[5] Thus, with increasing the thickness of the InSe spacer, the electron tunneling probability decreases exponentially, resulting in the disappearance of the MR.
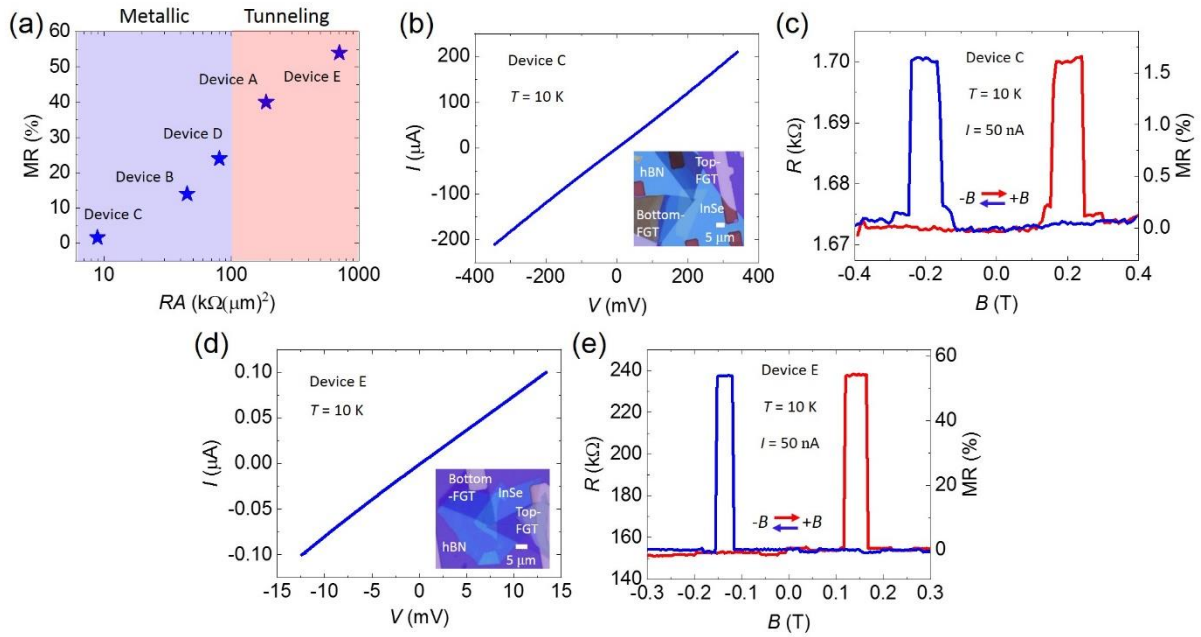


Figure S5. a) The MR as a function of the resistance-area product ($RA$) of devices with 6-nm-thick InSe. According to the $I$-$V$ characteristics of the devices (device A-E), they show metallic (left blue region) and tunneling (right red region) behaviors. b) $I$-$V$ curve of device C in parallel state indicates a linear metallic behavior. The inset shows the optical image of device C. c) $R$-$B$ curve of device C measured at a bias current of 50 nA, indicates a MR of ~1.6%. d) $I$-$V$ curve of device E in parallel state indicates a nonlinear tunneling behavior. The inset shows the optical image of device E. e) $R$-$B$ curve of device E, measured at a bias current of 50 nA, indicates a MR of ~54%. Red and blue horizontal arrows represent the sweeping directions of the magnetic field. The temperature is fixed at 10 K.

Figure S5a shows the MR as a function of the resistance-area product ($RA$) of the spin-valve devices with 6-nm-thick InSe. According to the $I$-$V$ characteristics of the devices (device

A-E), they shows metallic (left blue region) or tunneling (right red region) behaviors. The $RA$ value of tunneling devices is several to dozens of times larger than that of metallic devices. The devices B-D in the left blue region have smaller $RA$ values and the MR ratios suggest that pinholes may exits and that the transport mechanism is dominated by the giant MR effect. The existence of pinholes in InSe layer leads to the formation of a direct contact between top and bottom FGT electrodes, which consequently decreases the resistance of the device and the spin-injection efficiency. In contrast, the devices A and E in the right red region have larger $RA$ values and MR ratios, indicating Schottky barriers are formed at FGT/InSe interfaces. The transport mechanism of the devices is dominated by the tunneling MR effect. This indicates that pinholes have an important influence on the $RA$ and MR of the devices. As an example, Figure S5b shows the *I-V* curve of device C in parallel state indicating a linear metallic behavior. The *R-B* curve of device C measured at a bias current of 50 nA indicates a MR of ~1.6% (Figure S5c). In contrast, the *I-V* curve of device G in parallel state indicates a tunneling behavior (Figure S5d). Figure S5e shows the *R-B* curve of device E measured at a bias current of 50 nA, indicating a MR of 54%.

As shown in Figure S6a, the MR curve of device A measured at a negative bias current of -0.1 µA at 10 K gives a MR ratio of 40%. Figure S6b shows the MR curve of device B measured at a negative bias current of -1 µA at 10 K with a MR ratio of 14%. These two MR ratios are almost the same to the values of the positive counterpart, implying that the device possesses perfect up-down symmetry and two identical FGT/InSe van der Waals interfaces.
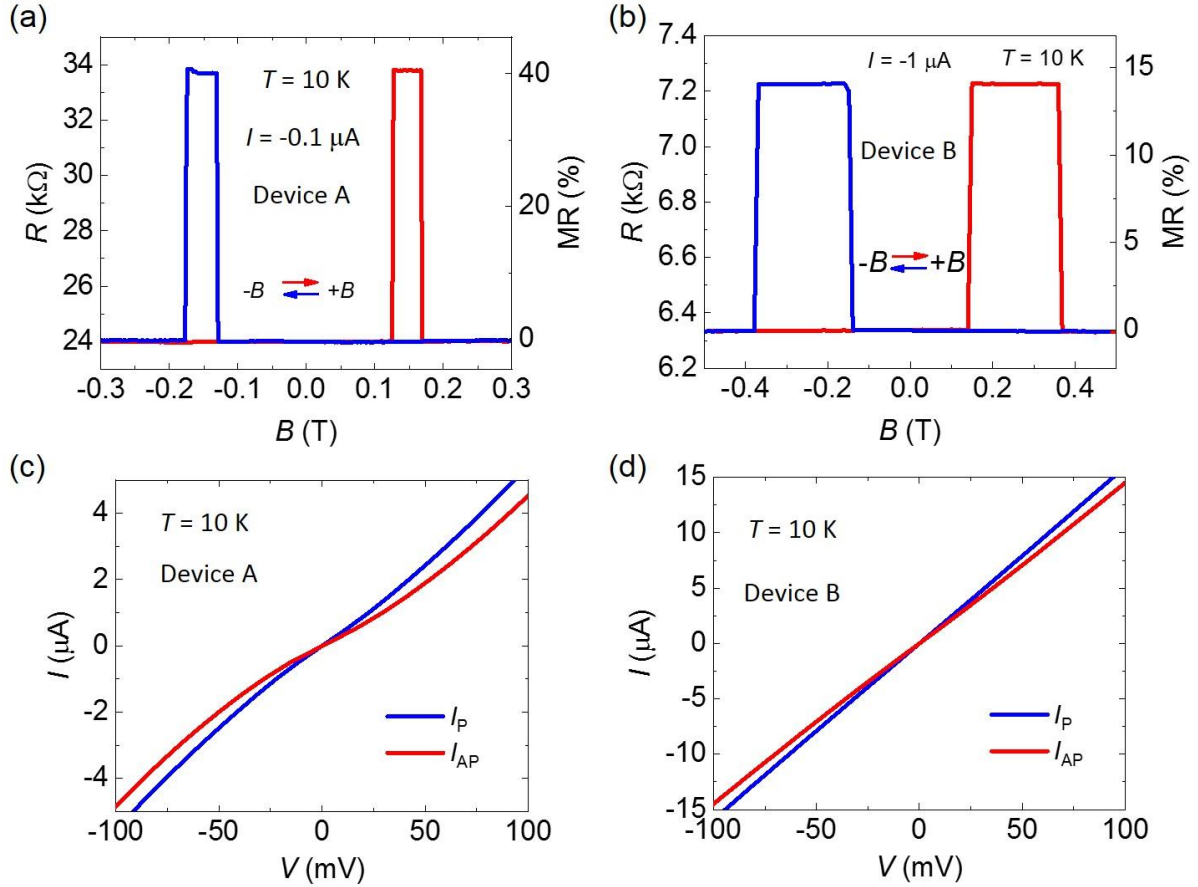
Figure S6. a) MR curve of device A measured at a negative bias current of -0.1 μA. b) MR curve of device B measured at a negative bias current of -1 μA. *I-V* curves measured in parallel and antiparallel magnetization configurations under zero magnetic field of c) device A and d) B at 10 K.

Before testing the electrical properties of the device, we first set the magnetization configurations between the top and bottom ferromagnetic electrodes to parallel or antiparallel alignments by an external magnetic field and then we set the external magnetic field back to zero. In both states, the system can keep their set states during the *I-V* measurements. The detailed process is as follows. First, we apply a large reverse magnetic field ($B_1$ = -0.4 T), which is larger than the coercivities of the top and bottom ferromagnetic electrodes ($B_1 > H_{c1} > H_{c2}$), so that the top and bottom ferromagnetic electrodes of the device are in the parallel alignment, and then set the magnetic field to zero. At this time, by testing the *I-V* curve, we obtain the electrical properties of the device in parallel state. Next, we apply a fixed forward magnetic field ($B_2$ = +0.15 T for device A or $B_2$ = +0.2 T for device B, $H_{c1} > B_2 > H_{c2}$), then the device

is in the antiparallel alignment, and finally we set the magnetic field back to zero. Similarly, by testing the *I-V* curve under this condition, we get the electrical properties of the device in the antiparallel state. Figure S6c-d shows the *I-V* curves measured in the parallel and antiparallel magnetization configurations under zero magnetic field at 10 K of device A and B, respectively. The obviously different resistance states of the two pairs of *I-V* curves demonstrate the nonvolatile characteristic of the two different magnetic configurations.

**References for Supporting Information**

[1]  D. A. Bandurin, A. V. Tyurnina, G. L. Yu, A. Mishchenko, V. Zólyomi, S. V. Morozov, R. K. Kumar, R. V. Gorbachev, Z. R. Kudrynskyi, S. Pezzini, Z. D. Kovalyuk, U. Zeitler, K. S. Novoselov, A. Patanè, L. Eaves, I. V. Grigorieva, V. I. Fal'ko, A. K. Geim, Y. Cao, *Nat. Nanotechnol.* **2017**, *12*, 223.

[2]  M. R. Molas, A. V. Tyurnina, V. Zólyomi, A. K. Ott, D. J. Terry, M. J. Hamer, C. Yelgel, A. Babiński, A. G. Nasibulin, A. C. Ferrari, V. I. Fal'ko, R. Gorbachev, *Faraday Discuss.* **2021**, *227*, 163.

[3]  H.-J. Deiseroth, K. Aleksandrov, C. Reiner, L. Kienle, R. K. Kremer, *Eur. J. Inorg. Chem.* **2006**, *2006*, 1561.

[4]  A. F. May, S. Calder, C. Cantoni, H. Cao, M. A. McGuire, *Phys. Rev. B* **2016**, *93*, 014411.

[5]  L. Zhang, T. Li, J. Li, Y. Jiang, J. Yuan, H. Li, *J. Phys. Chem. C* **2020**, *124*, 27429.